CHAPTER 3

BIDENTATE [N, O]-DONOR SALICYLALDIMINE SCHIFF BASE COMPLEXES OF OXOVANADIUM(IV) AND COPPER(II)

CHAPTER 3

BIDENTATE [N, O]-DONOR SALICYLALDIMINE SCHIFF BASE COMPLEXES OF OXOVANADIUM(IV) AND COPPER(II)

3.1 Introduction:

Schiff base complexes have received significant attention owing to their promising physico-chemical properties, bioactivities and catalytic properties in organic and inorganic transformations.[1-6] Metal complexes derived from Schiff base ligands feature amongst the earliest and most widely studied classes of metallomesogens.[7-9] The advantages of incorporating the imine functionality lie in the diverse range of potential structures and their ease of preparation.The salicylaldimine fragment is well recognised as a good promesogenic unit as the azomethine linkage is stabilized by intramolecular hydrogen bonding in addition to being a good donor site for coordination with metals.[10] The design and synthesis of paramagnetic complexes associated with multifunctional properties such as magnetic, electronic, or mesogenic properties desirable for technological applications is quite a challenging task for synthetic chemists.[11-15] The liquid crystalline behaviour of an organic compound is essentially dependent on its molecular architecture in which a slight change in its molecular geometry brings about considerable variation in its mesomorphic properties.[16,17] The majority of the metallomesogens based on salicylaldimine fragments that have been reported so far possess an alkyl or alkoxy tail on either side of the aromatic rings.[18-22] However, metallomesogens of salicylaldimine type ligands with polar substituents have not been adequately addressed.[23-25] The effect of polar substituents in a variety of mesogenic systems has been sporadically investigated during recent years. Introducing a lateral polar substituent at the aromatic core plays key role in phase behaviour.[26-28] Recognition of great potential of metallomesogens as advanced molecular materials led to a steady increase in interest toward liquid crystals incorporating transition metal elements.[29,30] Salicylaldiminato complexes have been synthesized using different metal ions such as copper(II), nickel(II), palladium(II) and iron.[31-39] Owing to unusual geometries and paramagnetism leading to unique

functional behaviours, metallomesogens incorporating VO(IV) metal ions is a focal theme of current research.[40-43] Mesophase formation depends mainly on the intermolecular interactions between ligand groups and their arrangements around metal ions.[44] Oxovanadium(IV) complexes owing to the presence of axial coordinative interaction have provided an additional control on the liquid crystalline behaviour over and above the variation in the flexibility of ligand tails.[40,41] Liquid crystals with transition metal core groups such as VO(IV) are a fascinating branch of material science, because the self-assemblies of coordinated metal complexes with new functionalities widen the range of potential applications.[44]

In this chapter we report a series of synthesis of oxovanadium(IV) and copper(II) complexes with bidentate [N,O]-donor Schiff base ligand containing lateral polar groups and a series of liquid crystalline oxovanadium(IV) Schiff base complexes containing both shorter as well as longer alkoxy substituent on either side of the ligand.

3.2 Experimental:

3.2.1 Synthesis of copper(II)/oxovanadium(IV) complexes from bidentate [N,O]-donor polar Schiff base ligands:

The general preparative route for salicylaldimine based Schiff bases metal complexes are presented in **Scheme 1**. The two step procedure involves alkylation of 2, 4-dihydroxybenzaldehyde followed by condensation with p-chloro or p-nitro substituted aniline. The vanadyl(IV) complexes, VOL_2 (L = salicylaldimines) were synthesized by the interaction of hot ethanolic solution of the ligands and vanadyl sulphate in the presence of triethylamine under reflux. The copper (II) complexes, CuL_2 (L=salicylaldimines) were synthesized by the interaction of hot ethanolic solution of the ligands and copper acetate at room temperature.

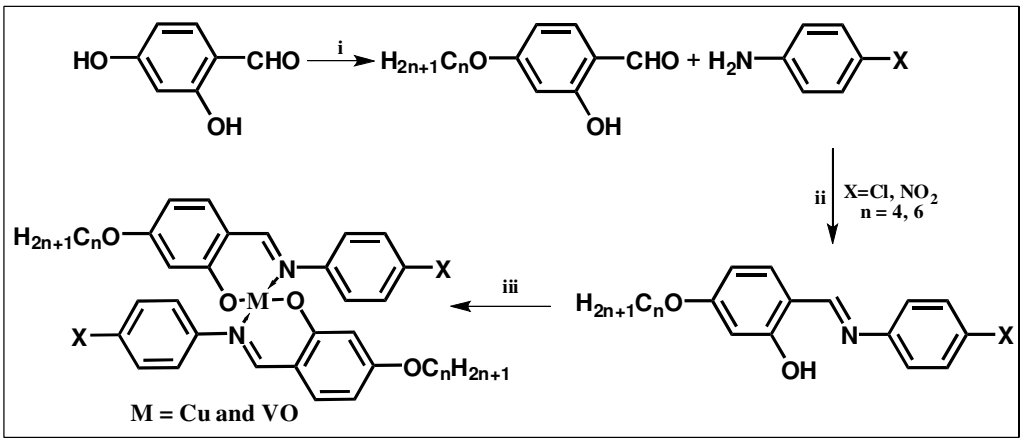

Scheme 1: i.$C_nH_{2n+1}Br$, $KHCO_3$, KI, dry acetone, Δ, 40h **ii.** Glacial AcOH, absolute EtOH Δ, 4h **iii.** $Cu(OAc)_2.2H_2O$/ $VOSO_4.2H_2O$, MeOH, TEA, Δ, 1h.

Synthesis of 4-n-alkoxysalicylaldehyde (n = 4, 6):

2,4-dihydroxybenzaldehyde (2.7g, 20mmol), potassium bicarbonate(2g, 20mmol), potassium iodide(catalytic amount) and 1-bromobutane (2.7g, 20mmol) or 1-bromohexane (3.2g, 20mmol) were mixed in 400 cm^3 dry acetone. The mixture was refluxed for 40 h and filtered when hot to remove insoluble solids. Dilute hydrochloric acid was added to neutralize the warm solution, which is then extracted twice with $CHCl_3$. The combined $CHCl_3$ extract was concentrated to give a purple solid. The solid was purified by column chromatography with silica gel (100-200) mesh with a mixture of hexane: $CHCl_3$ (1:1).The solvent was evaporated to give a white solid product.

Synthesis of N-(4-n-butyloxysalicylidene)-4′-4-chlroaniline(4-Cl):

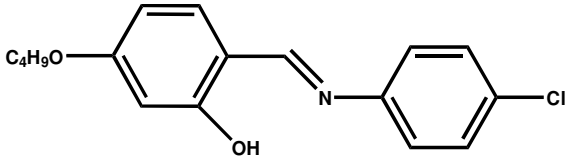

An ethanolic solution of (4-n-butyloxy)-salicyldehyde (0.19g, 1mmol) was added to an ethanolic solution of 4-chloroaniline (0.12g, 1mmol). The solution mixture was refluxed for 3h with few drops of acetic acid as catalyst to yield the Schiff base N-(4-n-butyloxysalicylidene)-4′-n-chloroaniline. The solid was collected by filtration and recrystallised several times from absolute ethanol to give a pure compound.

Yield: 0.23g (75%); m.p., 118°C. FAB Mass (m/e, fragment): m/z: calc. 303.1; found: 304.1[M+H$^+$]; Anal. Calc. for $C_{17}H_{18}ClNO_2$(303.1): C, 67.21; H, 5.97; N 4.61. Found: C, 67.22; H, 5.95; N, 4.62%. ^{1}H NMR (400 MHz, $CDCl_3$): δ 0.88(t, J = 6.8Hz, 3H, CH_3), 0.93-1.8 (m, 4H, $(-CH_2)_2$, 3.95(t, J = 6.7Hz, 2H, $-OCH_2$), 7.3(d, J=7.2, 1H, H-aryl), 8.21(s, 1H, CH=N), 13.7(s, 1H, OH). IR (ν_{max}, cm^{-1}, KBr):3435(ν_{OH}), 2917($\nu_{as(C-H),}$ CH_3), 2879($\nu_{s(C-H),}$ CH_3), 1631($\nu_{C=N}$), 1277(ν_{C-O}).

Synthesis of N-(4-n-hexyloxysalicylidene)-4′-6-chlroaniline (6-Cl):

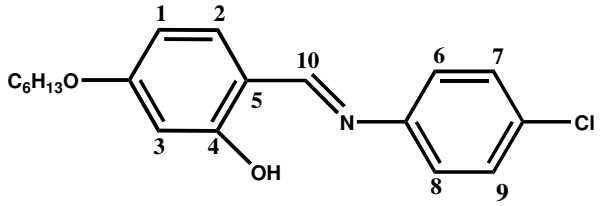

Yield: 0.24g (70%); m.p., 122^{0}C. FAB Mass (m/e, fragment): m/z: calc. 331.1; found: 332.1 [M+H$^+$]; Anal. Calc. for $C_{19}H_{22}ClNO_2$(331.1): C, 68.77; H, 6.68; N 4.22. Found: C, 68.72; H, 6.65; N, 4.23%. ^{1}H NMR (400 MHz, $CDCl_3$): δ 0.88(t, J = 6.8Hz, 3H, CH_3), 0.94-1.7 (m, 4H, $(-CH_2)_4$, 3.94(t, J = 6.6Hz, 2H, $-OCH_2$), 7.4(d, J=7.1, 1H, H-aryl), 8.22(s, 1H, CH=N), 13.8(s, 1H, OH). ^{13}C NMR (75.45 MHz; $CDCl_3$; Me_4Si at 25°C, ppm) δ= 106.3 (-C1), 131.1 (-C2), 104.9 (-C3), 161.6 (-C4), 109.3 (-C5), 122.7 (-C6), 132.1(-C7), 122.6 (-C8), 131.4 (-C9), 159.8(-C10). IR (ν_{max}, cm^{-1}, KBr):3434(ν_{OH}), 2918($\nu_{as(C-H),}$ CH_3), 2874($\nu_{s(C-H),}$ CH_3), 1632($\nu_{C=N}$), 1276(ν_{C-O}).

Synthesis of N-(4-n-butyloxysalicylidene)-4′-4-nitroaniline (4-NO_2):

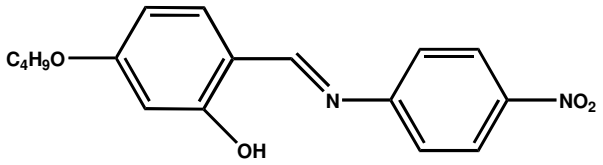

Yield: 0.25g (75%); m.p., 116°C. FAB Mass (m/e, fragment): m/z: calc. 314.1; found: 315.1 [M+H$^+$]; Anal. Calc. for $C_{17}H_{18}N_2O_4$(314.1): C, 64.96; H, 5.77; N 8.91. Found: C, 64.95; H, 5.75; N, 8.92%. ^{1}H NMR (400 MHz, $CDCl_3$): δ 0.96(t, J = 6.8Hz, 3H, CH_3), 0.94-1.7 (m, 4H, $(-CH_2)_2$), 3.94(t, J = 6.6Hz, 2H, $-OCH_2$), 7.4(d, J=7.1, 1H, H-aryl), 8.22(s, 1H, CH=N), 13.8(s, 1H, OH). IR (ν_{max}, cm^{-1}, KBr):3434(ν_{OH}), 2918($\nu_{as(C-H)}$, CH_3), 2874($\nu_{s(C-H)}$, CH_3), 1632($\nu_{C=N}$), 1276(ν_{C-O}), 1516($\nu_{as(NO)}$), 1350(($\nu_{s(NO)}$),.

Synthesis of N-(4-n-hexyloxysalicylidene)-4′-6-nitroaniline (6-NO_2):

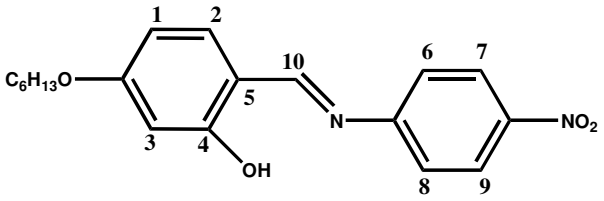

Yield: 0.25g (75%); m.p.122°C. FAB Mass (m/e, fragment): m/z: calc. 342.1; found: 343.1 [M+H^+]; Anal. Calc. for $C_{19}H_{22}N_2O_4$(342.1): C, 64.96; H, 5.77; N 8.91. Found: C, 66.65; H, 6.48; N, 8.18%. ^{1}H NMR (400 MHz, $CDCl_3$): δ 0.94(t, J = 6.7Hz, 3H, CH_3), 0.92-1.8 (m, 4H, (-CH_2)4, 3.93(t, J = 6.5Hz, 2H, -OCH_2), 7.53(d, J=7.1, 1H, H-aryl), 8.21(s, 1H, CH=N), 13.8(s, 1H, OH). 13C NMR (75.45 MHz; $CDCl_3$; Me_4Si at 25°C, ppm) δ= 107.2 (-C1), 130.1 (-C2), 102.4 (-C3), 161.5 (-C4), 109.8 (-C5), 122.9 (-C6), 122.3(-C7), 123.6 (-C8), 122.4 (-C9), 147.8(-C10). IR (ν_{max}, cm^{-1}, KBr):3434(ν_{OH}), 2918($\nu_{as(C-H),}$ CH_3), 2876($\nu_{s(C-H),}$ CH_3), 1632($\nu_{C=N}$), 1276(ν_{C-O}), 1517($\nu_{as(NO)}$), 1352($\nu_{s(NO)}$).

Synthesis of copper(II) complexes (Cu-n-X, n = 4, 6 and X = Cl, NO_2):

The ligand 4-Cl (0.30g, 1mmol) or 6-Cl (0.33g, 1mmol) or 4-NO_2 (0.31g, 1mmol) or 6-NO_2 (0.34g, 1mmol) was dissolved in minimum volume of absolute ethanol and copper acetate $Cu(OAc)_2$. H_2O (0.09g, 0.5mmol) in methanol was then added slowly and stirred for 2h at room temperature. A brown solid formed immediately was filtered, washed with diethyl ether and recrystallized from chloroform-ethanol (1:1).

Cu-4-Cl:

Yield: 0.29g (75%); m.p., 237°C. FAB Mass (m/e, fragment): m/z: calc. 669.1; found: 670.1 [M+H^+]; Anal. Calc. For $C_{34}Cl_2H_{34}CuN_2O_4$(669.1): C, 61.03; H, 5.12; N 4.19. Found: C, 61.02; H, 5.13; N, 4.18%. IR (ν_{max}, cm^{-1}, KBr): 2914($\nu_{as(C-H),}$ CH_3), 2874($\nu_{s(C-H),}$ CH_3), 1611($\nu_{C=N}$), 1274(ν_{C-O}).

Cu-6-Cl:

Yield: 0.31g (76%); m.p., 227°C. FAB Mass (m/e, fragment): m/z: calc. 725.1; found: 726.1 [M+H^+]; Anal. Calc. for $C_{38}H_{42}Cl_2CuN_2O_4$(725.1): C, 62.94; H, 5.84; N 3.86. Found: C, 61.92; H, 5.83; N, 3.85%. IR (ν_{max}, cm^{-1}, KBr): 2914($\nu_{as(C-H),}$ CH_3), 2874($\nu_{s(C-H),}$ CH_3), 1612($\nu_{C=N}$), 1274(ν_{C-O}).

Cu-4-NO_2:

Yield: 0.30g (75%); m.p., 237°C. FAB Mass (m/e, fragment): m/z: calc. 689.1; found: 690.1 [M+H^+]; Anal. Calc. For $C_{34}H_{34}CuN_4O_8$(689.1): C, 59.17; H, 4.97; N 8.12. Found: C, 59.18; H, 4.99; N 8.15%. IR (ν_{max}, cm^{-1}, KBr): 2915($\nu_{as(C-H),}$ CH_3), 2875($\nu_{s(C-H),}$ CH_3), 1611($\nu_{C=N}$), 1276(ν_{C-O}).

Cu-6-NO_2:

Yield: 0.31g (76%); m.p., 227°C. FAB Mass (m/e, fragment): m/z: calc. 745.23; found: 746.24 [M+H^+]; Anal. Calc. for $C_{38}H_{42}CuN_4O_8$(745.23): C, 61.16; H, 5.67; N 7.51. Found: C, 61.26; H, 5.60; N, 7.50%. IR (ν_{max}, cm^{-1}, KBr): 2916($\nu_{as(C-H),}$ CH_3), 2876($\nu_{s(C-H),}$ CH_3), 1612($\nu_{C=N}$), 1275(ν_{C-O}).

Synthesis of oxovanadium(IV) complexes (VO-n-X, n = 4, 6 and X = Cl, NO_2):

The ligand 4-Cl (0.30g, 1mmol) or 6-Cl (0.33g, 1mmol) or 4-NO_2 (0.31g, 1mmol) or 6-NO_2 (0.34g, 1mmol) was dissolved in minimum volume of absolute ethanol and vanadyl sulphate, $VOSO_4.5H_2O$ (0. 12g, 0.5mmol) dissolved in methanol was added to it followed by addition of triethylamine and refluxed for 2h. A greenish solid formed immediately was filtered, washed with diethyl ether and recrystallized from chloroform-ethanol.

VO-4-Cl:

Yield=0.31g, 75%. *Anal*. Calc. for $C_{34}H_{34}Cl_2N_2O_5V$ (671.1): C, 60.72; H, 5.10; N, 4.17. Found: C, 60.71; H, 5.11; N, 4.16%; FAB Mass (m/e, fragment): m/z: calc. 671.1; found: 672.1[M+H^+]. IR (ν_{max}, cm^{-1}, KBr): 2912($\nu_{as(C-H),}$ CH_3), 2873($\nu_{s(C-H),}$ CH_3), 1612($\nu_{C=N}$), 981($\nu_{V=O}$).

VO-6-Cl:

Yield = 0.31g, 70%. *Anal*. Calc. for $C_{38}H_{42}Cl_2N_2O_5V$ (727.1): C, 62.64; H, 5.81; N, 3.84. Found: C, 62.63; H, 5.82; N, 3.85%; FAB Mass (m/e, fragment): m/z: calc. 727.1; found: 728.1[M+H^+]. IR (ν_{max}, cm^{-1}, KBr): 2916($\nu_{as(C-H),}$ CH_3), 2877($\nu_{s(C-H),}$ CH_3), 1615($\nu_{C=N}$), 982($\nu_{V=O}$).

VO-4-NO_2:

Yield = 0.32g, 76%. *Anal*. Calc. for $C_{34}H_{34}N_4O_9V$ (693.1): C, 58.88; H, 4.94; N, 8.08. Found: C, 58.86; H, 4.93; N, 8.07%; FAB Mass (m/e, fragment): m/z: calc. 693.1; found: 694.1[M+H^+]. IR (ν_{max}, cm^{-1}, KBr): 2917($\nu_{as(C-H),}$ CH_3), 2876($\nu_{s(C-H),}$ CH_3), 1613($\nu_{C=N}$), 981($\nu_{V=O}$).

VO-6-NO_2:

Yield = 0.34g, 75%. *Anal*. Calc. for $C_{38}H_{42}N_4O_9V$ (749.2): C, 60.88; H, 5.65; N, 7.47. Found: C, 60.87; H, 5.64; N, 7.46%; FAB Mass (m/e, fragment): m/z: calc. 749.2; found: 750.2[M+H^+]. IR (ν_{max}, cm^{-1}, KBr): 2918($\nu_{as(C-H),}$ CH_3), 2876($\nu_{s(C-H),}$ CH_3), 1610($\nu_{C=N}$), 983($\nu_{V=O}$).

3.2.1.1 Results and Discussion:

Synthesis and structural assessment:

Synthesis of the compounds was carried out following a procedure (Scheme 1) similar to that reported earlier for related systems.[23,40] The ligands [N, N′-bis-(4-X-amino phenyl (4′-n-alkoxy)-salicylaldiminato)] are hereafter abbreviated as n-X,where n indicates the number of carbon atoms in alkoxy chains, n = 4, 6; X=Cl, NO_2 and their Cu(II), VO(IV) complexes (Cu-n-X⁄VO-n-X). The compounds were characterized by ^{1}H NMR, ^{13}CNMR, FT-IR, UV-Vis spectroscopy, FAB mass spectroscopy and elemental analysis. Solution electrical conductivity measurements in CH_2Cl_2 revealed non-ionic nature of the complexes. Infrared (IR) spectra of the complexes showed a shift of ν_{CN} vibrational stretching frequency at ca. 1625cm^{-1} to a lower wave number ($\Delta\nu$ ~30cm^{-1}) and absence of ν_{OH} mode and phenolate oxygen upon chelation, clearly suggesting the coordination of azomethine-N and phenolate-O to the metal. The $\nu_{C=N}$ stretching frequency is rather independent of the length of alkoxy side chain in both ligands and their complexes. The vanadyl(V=O) stretching at ca. 980cm^{-1} is suggestive of the absence of any intermolecular (.....V=O.....V=O.....) interaction, indicating the monomeric nature of the complexes. The presence of linear chain interactions usually causes $\nu_{V=O}$ to shift to a lower wave number (ca. 870cm^{-1}). The IR data also showed the V=O stretching frequency to be insensitive to the length of the alkoxy side chain. Moreover, two weak bands in the low-energy region (400-600cm^{-1}) assignable to $\nu_{(M-N)}$ and $\nu_{(M-O)}$ provide compelling evidence for the coordinated metal ion in the ligand framework.

Photophysical Study:

The ultraviolet-visible (UV-Vis) absorption spectra (**Fig.1**) of the ligands consists of an intense band centred at ~344-372nm attributed to π-π* transitions of the azomethine group. Another weak band (at ~288-291nm) in the higher energy region

was due to π-π* transitions of benzene rings. Upon complexation these bands are red shifted (**Fig.2 and Fig.3**). The UV-Vis data are summarised in Table 1. Photoluminescence studies of the compounds were carried out at room temperature in the solid state (**Fig. 4**). The ligands emit green light at 538nm (Φ = 12%) for chloro-substituted compounds and at 559nm (Φ = 9%) for the nitro-substituted ones when excited at 330nm. The solid state emission spectrum of the complex was recorded by placing a uniform powder sheet between two quartz plates. The λ_{max} values of all the nitro-substituted compounds are red shifted owing to the electron-withdrawing nature of the $-NO_2$ group. The Schiff bases exhibit fluorescence due to intraligand (π-π*) transitions.[45] Complexes did not exhibit any emission, presumably because paramagnetic ions quench the fluorescence of organic ligands by enhancing the rate of non-radiative processes (intersystem crossing, etc.) that compete with fluorescence.[46, 47] It may be noted that quenching of fluorescence of a ligand by paramagnetic metal ions on complexation is a rather usual phenomenon which is explained by processes such as magnetic perturbation, redox-activity, electronic energy transfer, etc.

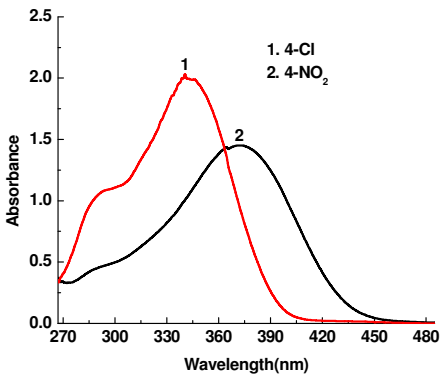

Fig. 1. UV-visible spectra of 4-Cl and $4\text{-}NO_2$

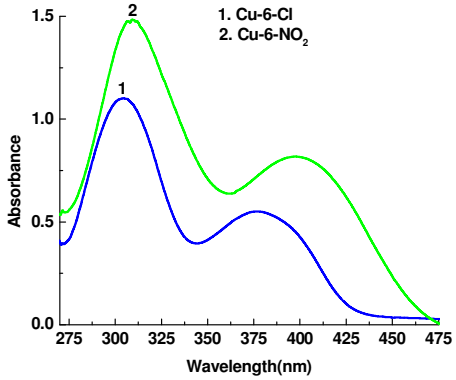

Fig. 2. UV-visible spectra of Cu-6-Cl and $Cu\text{-}6\text{-}NO_2$

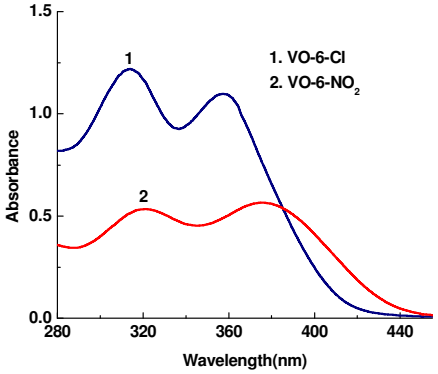

Fig. 3. UV-visible spectra of VO-6-Cl and VO-6-NO_2

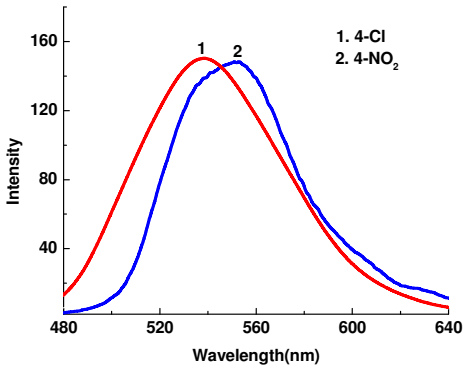

Fig. 4. Photoluminescence spectra of 4-Cl and 4-NO_2

Table 1: UV-visible and photoluminescence data of ligands and complexes

Compounds	**$\pi\rightarrow\pi^*$ (ε, l mol^{-1} cm^{-1})**	**PL[a] (Solid)**
4-Cl	290(11300)	538
	342(14200)	
VO-4-Cl	314(11200)	-
	358(14100)	
Cu-4-Cl	305(12200)	-
	378(13200)	
6-Cl	292(11400)	541
	343(14300)	
VO-6-Cl	313(12200)	-
	354(14100)	
Cu-6-Cl	304(12400)	-
	377(13400)	
4-NO_2	294(4700)	554
	374(14500)	
VO-4-NO_2	323(5200)	-
	379(5400)	
Cu-4-NO_2	312(14300)	-
	401(8100)	
6-NO_2	295(4600)	559
	377(14400)	
VO-6-NO_2	326(5300)	-
	381(5200)	
Cu-6-NO_2	314(14200)	-
	406(8200)	

[a] **Photoluminescence data.**

Cyclovoltammetry Study:

The redox behaviour for Cu-6-NO_2/VO-6-NO_2 complexes was probed by cyclic voltammetry in dichloromethane solution in the potential range -4.0-1.4V versus SCE electrode at a scan rate of 0.05Vs^{-1}. The voltamogram (**Fig.5**) displayed a quasireversible (peak separation>100mV) one-electron response. The peak separation ($E_{1/2}$ = +0.453 E_p^c = -0.485V, E_p^a = -0.385V, E_p = 0.100V) is assigned to the Cu(II) / Cu(I) couple. The electrochemical behaviour of the vanadium complex (VO-6-NO_2) also displayed a quasireversible (peak-to-peak separation>100mV) cyclic voltammetric response due to the VO^{3+} / VO^{2+} couple at ($E_{1/2}$= +0.605V, E_p^c = 0.391V, E_p^a = 0.822V, E_p = 0.431V).

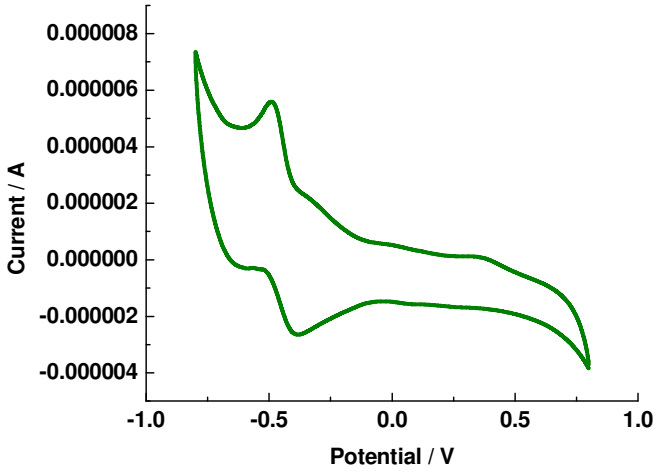

Fig. 5: Cyclic voltammogram of Cu-6-NO_2

Variable temperature magnetic susceptibility study:

The effective magnetic moments of the complex VO-6-NO_2 and Cu-6-NO_2 were found to be 1.72B.M (d^1) and 1.81B.M (d^9), respectively. The inverse magnetic susceptibility for a representative complex, VO-6-NO_2, is plotted against temperature (**Fig.6**), satisfying the Curie–Weiss equation. The effective magnetic moment did not vary appreciably in the range of experimental temperature.

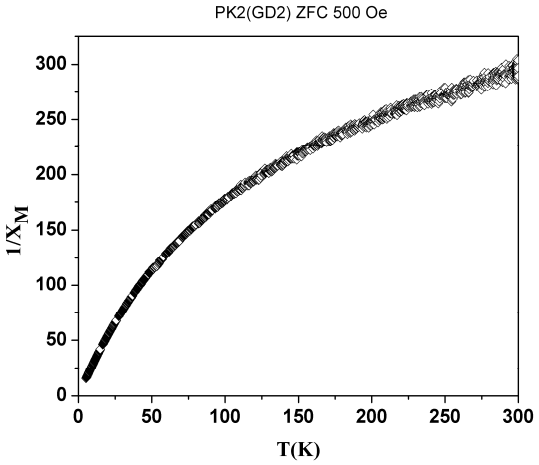

Fig. 6: Variation of inverse magnetic susceptibility of VO-6-NO_2 with temperature

Mesomorphic properties:

The mesomorphic properties of the compounds were investigated using polarised optical microscopy and differential scanning calorimetry study. The phase transitions and thermodynamic data are summarized in Table 2. The formation of mesophases is strongly dependent on the electronic and/or the steric factors of the substituents. Compound 4-NO_2 was found to be non-mesogenic. However, 4-Cl compound showed enantiotropic SmA mesophase. The compound melts to isotropic liquid at 118°C. Upon cooling the sample a highly birefringent fanlike texture is formed, which is characteristic of the SmA phase (**Fig.7**). The DSC trace (**Fig.8**) showed three transitions in heating and two in cooling cycle. The compound is thermally quite stable. Though a crystal to crystal phase transition was encountered in DSC, in POM study this could not be detected. Quite different trend, however, was observed for the 6-Cl and 6-NO_2 compounds. The compound 6-Cl compound exhibited SmA phase over a wide range of temperature. Surprisingly unlike other compounds being reported here, the compound 6-NO_2 showed a nematic phase (N), (**Fig.9**) with a very low enthalpy value (ΔH = 0.81kJmol^{-1}). The DSC traces (**Fig.10**) showed two transitions both in heating and cooling cycles. We have no suitable explanation for this behaviour at this stage. For the ligands, both melting point and clearing point of chloro substituted compounds is about 30°C higher than the nitro substituted compound. The melting temperatures of the complexes were always substantially

higher than the ligands. When nitro substituted the mesomorphism was upset in complexes with n = 4 carbon chain length. Copper complexes are all found to be mesogenic and revealed a SmA phase (**Fig.11**) at ~200-225°C. Owing to the high viscous nature of the compound and severe restriction in the molecular mobility, a pronounced hysteresis in transition temperature has been noted. Among the whole series of the complexes, only Cu-6-NO_2 exhibited enantiotropic mesomorphism with high thermal stability. The compounds Cu-4-Cl and Cu-6-Cl showed monotropic mesomorphism. The DSC thermogram for the typical compound Cu-6-NO_2 is shown in the (**Fig.12**). None of the vanadyl complexes showed any mesogenicity.

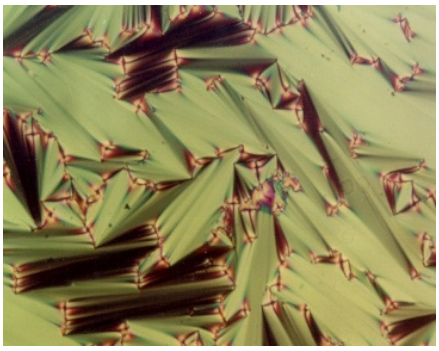

Fig. 7: Fan-like texture of SmA phase (4-Cl)

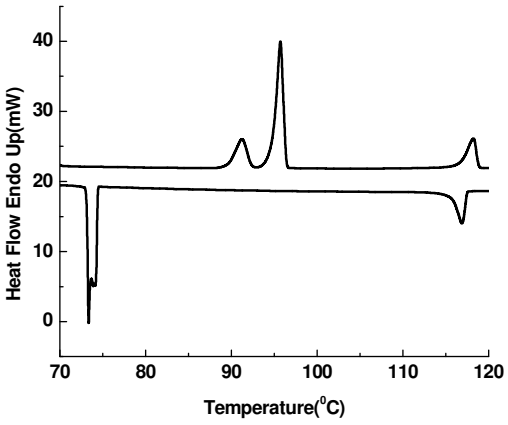

Fig. 8: DSC thermogram of (4-Cl)

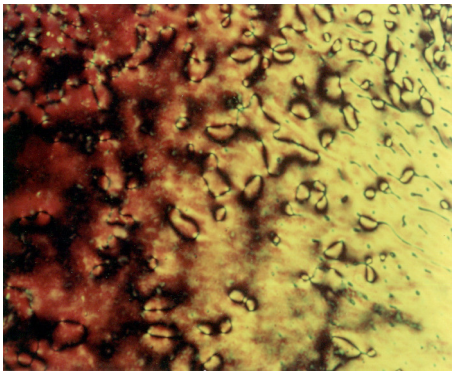

Fig. 9: Schlieren texture of N phase of (6-NO_2)

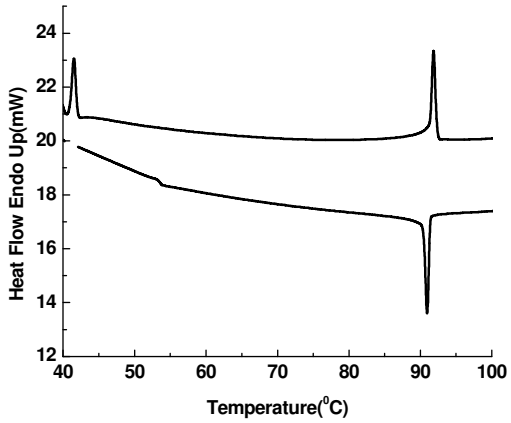

Fig. 10: DSC thermogram of 6-NO_2

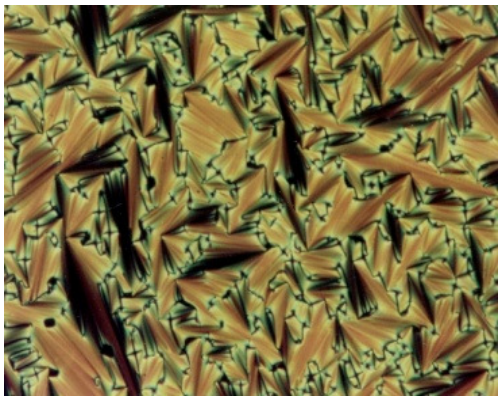

Fig. 11: Focal conic texture of SmA phase of (Cu-6-NO_2)

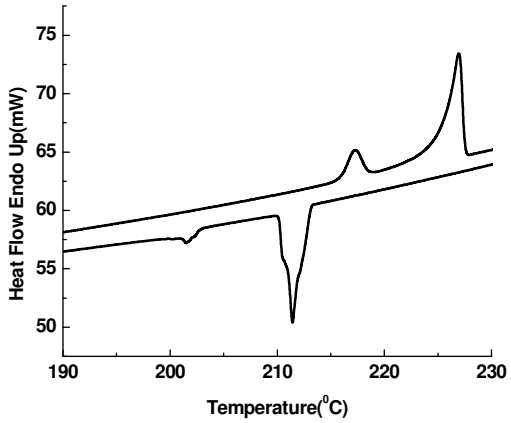

Fig. 12: DSC trace of Cu-6-NO_2

Table 2: Phase transitions temperatures (T°C), associated enthalpies (ΔH, $kJmol^{-1}$) of n-X and their complexes.

Compounds	Heating	Cooling
4-Cl	Cr93.2(7.5)Cr96(12.8)SmA 118.7(3.8)I	I 116.7(3.4)SmA71.8(6.0)Cr
4-NO_2	Cr 116.7 (7.9) I	I 56.8 (8.5) Cr
6-Cl	Cr 78.1 (15.6) SmA 122.6 (4.1) I	I 121.4 (3.9) SmA 47.4 (14.5)
6-NO_2	Cr 42.3(0.7)N92.6(0.7)I	I 91.5(0.8)N41.7(0.5)Cr
Cu-4-Cl	Cr 236.6(26.4) I	I 98.2(5.3)SmA193.7(1.6)Cr
Cu-4-NO_2	Cr 234.7(21.6) I	Cr 45.8(9.6) I
Cu-6-Cl	Cr 216.1(20.0) I	I 208.6(1.7) SmA 176.0(20.8)
Cu-6-NO_2	Cr 217.2(17.3)SmA227.0(71.2)I	I11.3(71.1)SmA201.4(4.7)Cr
VO-6-Cl	Cr 182.2(21.4)I	I68.1(14.2)Cr
VO-6-NO_2	Cr 178.2(12.4)I	I58.1(13.2)Cr

DFT study:

The first task for the density functional theory (DFT) calculation is to determine the lowest energy electronic structure of the representative compounds. Geometry optimizations and energy calculations of Cu-6-Cl (**Fig.13**), Cu-6-NO_2 (**Fig.14**), VO-6-Cl (**Fig.15**) and VO-6-NO_2 (**Fig.16**) complexes were performed using the unrestricted BLYP/DNP methods without imposing any symmetry constrain. The BLYP functional used, comprises of a hybrid exchange functional as defined by Becke and the non-local Lee–Yang–Parr correlation functional.[48] The basis set chosen in this study is DNP, the double-numerical atomic orbitals augmented by polarization functions. All calculations were performed with DMol3 program package.[49] The 3D

iso-surface plots of the lowest unoccupied molecular orbital (LUMO) and highest occupied molecular orbital (HOMO) of copper and vanadium complexes are shown in (**Fig.17-24**). The analysis of the wave function indicates that the electron absorption corresponds to the transition from the ground to the first excited state and is mainly described by one-electron excitation from the HOMO to the LUMO. In both the copper complexes, electron density of the HOMO is localized mainly on the aromatic rings bearing the alkoxy substituent while the LUMO is localized on and around the copper atom. The noticeable differences in the distribution of electron densities on the HOMO as well as LUMO of Cu-6-Cl and Cu-6-NO_2 complexes may be ascribed to the nature of different substituent on the aromatic rings. The molecular orbital energies of HOMO and LUMO of Cu-6-Cl are calculated to -5.149eV and -4.044eV, respectively, ΔE = 1.105eV. Corresponding energies for Cu-6-NO_2 complex have been found to be -5.563eV and -4.471eV, respectively, ΔE=1.092eV. It is also noticed from Figure 21-24, in the both the vanadium complexes, electron density of HOMO is localized on vanadium atom. The LUMO of VO-6-Cl is localized on V-N bond along with C=N double bond while LUMO of VO-6-NO_2 is concentrated mainly on –NO_2 substituent containing aromatic ring. The orbital energies of HOMO and LUMO of VO-6-Cl complex are evaluated to be -5.134eV and -3.244eV, respectively, ΔE = 1.890 eV. Corresponding energies for VO-6-NO_2 complex have been calculated to be -5.536eV and -3.769eV, respectively, ΔE= 1.767eV. A relatively lower HOMO and LUMO energy gap for copper and vanadium complexes explains the eventual charge transfer interactions taking place within the molecule. The lower energy differences also reflect the chemical activity of these copper and vanadium complexes. Hence, copper complexes are predictably more reactive than vanadium complexes. The chemical hardness values of Cu-6-Cl, Cu-6-NO_2, VO-6-Cl and VO-6-NO_2 complexes are evaluated to be 0.553, 0.546, 0.945 and 0.884eV, respectively, at BLYP/DNP level. The maximum hardness principle[50] states that the higher the hardness, the higher is the stability, i.e. lower is the reactivity. It is also noticed that introduction of –NO_2 substituent increases the reactivity of the copper and vanadium complexes. Some of the significant geometric parameters of optimized copper and vanadium complexes, evaluated by DFT calculation at BLYP/DNP level are shown in the Table 3 and Table 4 respectively. The Cu—O1, Cu—O2, Cu—N1 and Cu—N2 bond

lengths of Cu-6-Cl complex are 1.947, 1.946, 2.041 and 2.043Å, respectively, implying the presence of regular σ and dative bonding. The bond angles O1—Cu—O2, N1—Cu—N2, O1—Cu—N1 and O2—Cu—N2 around Cu atom are calculated to be 151.40, 147.70, 93.00 and 93.00, respectively, suggested slightly distorted square planar geometry. These geometrical parameters match well with related structurally characterized square planar copper complexes.[51] The bond angles of 127.60 and 163.40 for O1–V–O2 and N1–V–N2, respectively, in complex VO-6-Cl and 127.70 and 162.60 for O1–V–O2 and N1–V–N2, respectively in VO-6-NO_2 complex confirm a distorted square pyramidal geometry around the vanadyl(IV) centre.

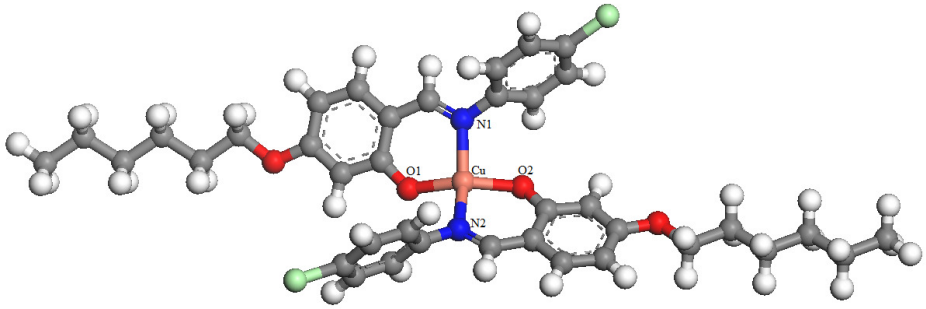

Fig. 13: Optimized structure of Cu-6-Cl

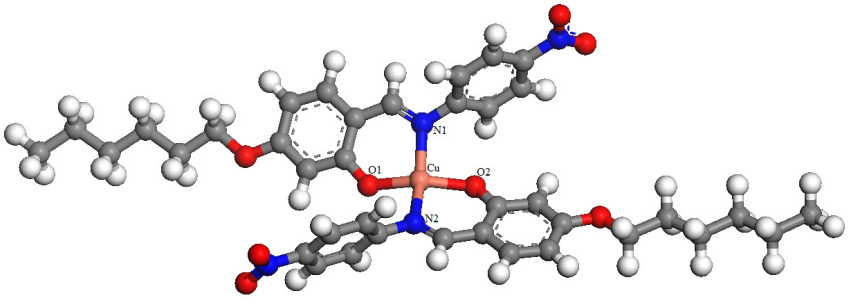

Fig. 14: Optimized structure of Cu-6-NO_2

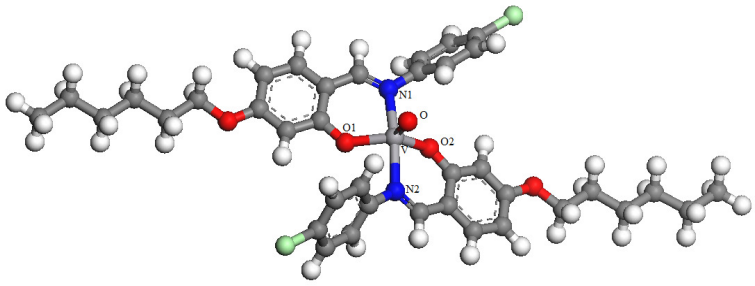

Fig. 15: Optimized structure of VO-6-Cl

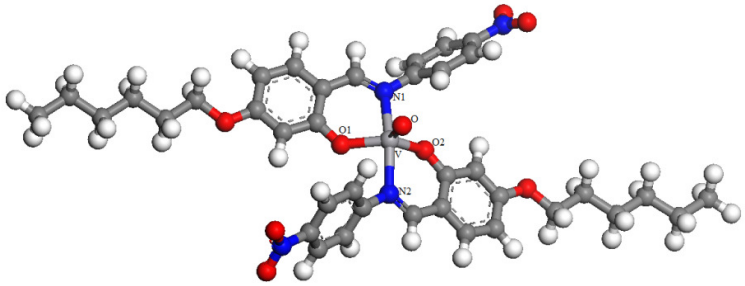

Fig. 16: Optimized structure of VO-6-NO_2

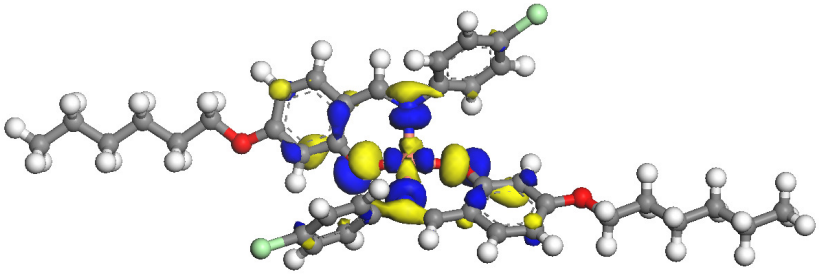

Fig. 17: HOMO of Cu-6-Cl

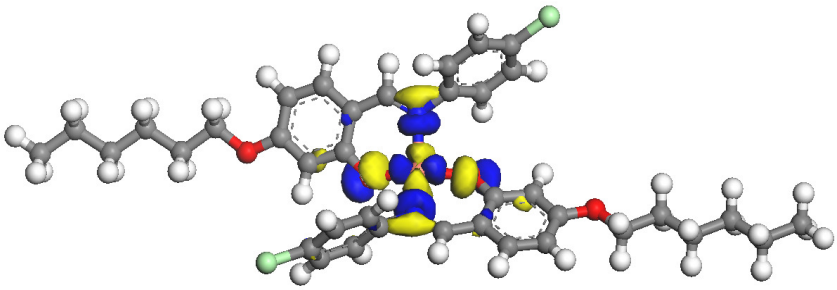

Fig. 18: LUMO of Cu-6-Cl

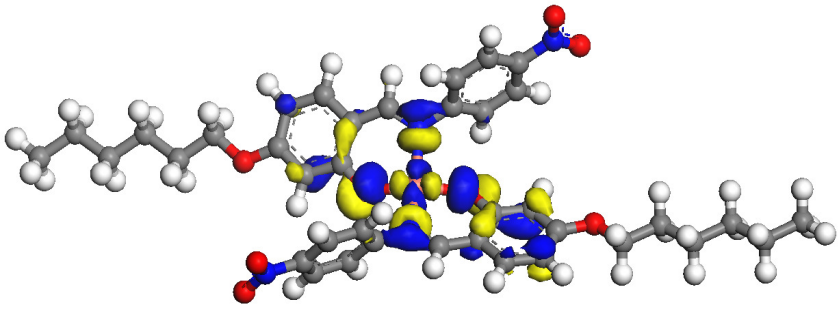

Fig.19: HOMO of Cu-6-NO_2

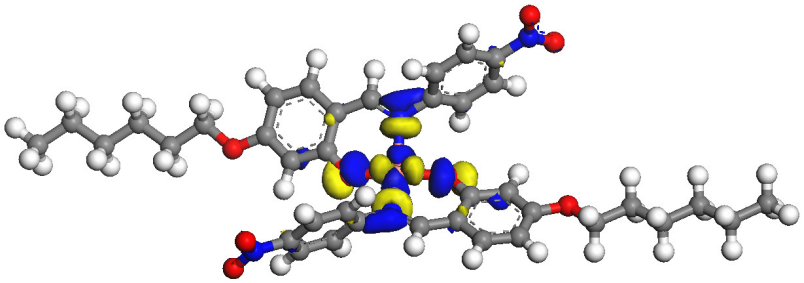

Fig. 20: LUMO of Cu-6-NO_2

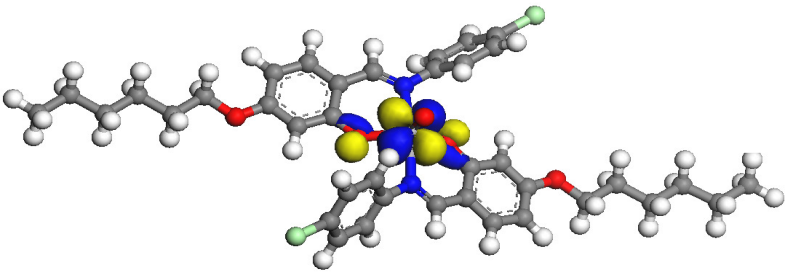

Fig. 21: HOMO of VO-6-Cl

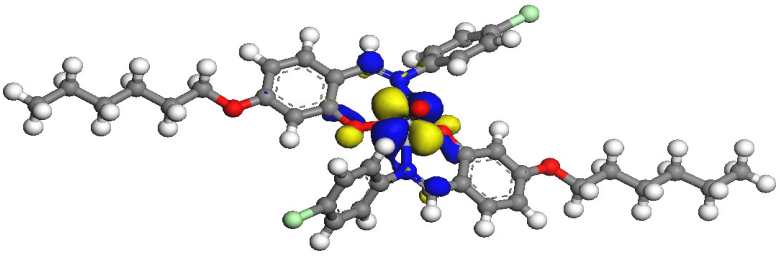

Fig. 22: LUMO of VO-6-Cl

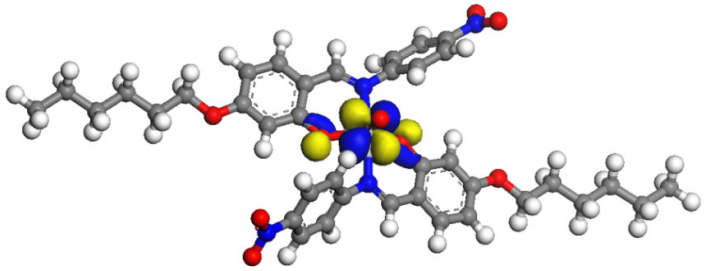

Fig.23: HOMO of VO-6-NO_2

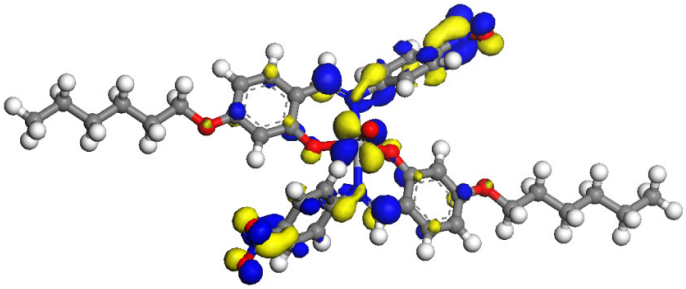

Fig. 24: LUMO of VO-6-NO_2

Table 3: Selected bond lengths (Å) and bond angles (°) of Cu-6-Cl and Cu-6-NO_2 complexes optimized at the BLYP/DNP level.

Structure parameter	Cu-6-Cl	Cu-6-NO_2
Cu—O1	1.947	1.941
Cu—O2	1.946	1.939
Cu—N1	2.041	2.047
Cu—N2	2.043	2.052
O1—Cu—O2	151.4	154.5
N1—Cu—N2	147.7	150.7
O1—Cu—N1	93.0	92.7
O2—Cu—N2	93.0	92.7

Table 4: Selected bond lengths (Å) and bond angles(°) of VO-6-Cl and VO-6-NO_2 complexes optimized at the BLYP/DNP level.

Structure parameter	VO-6-Cl	VO-6-NO_2
V—O1	1.950	1.944
V—O2	1.950	1.944
V—O	1.623	1.622
V—N1	2.175	2.178
V—N2	1.177	2.178
O1—V—O2	127.6	127.7
N1—V—N2	163.4	162.6
O1—V—N1	86.5	86.4
O2—V—N2	86.4	86.4

3.2.2 Synthesis of oxovanadium(IV) complexes of bidentate [N, O] donor Schiff base ligands:

The general preparative route for alkoxy salicylaldehydes is presented in **Scheme2**. The Schiff base ligands were synthesized by condensation of the appropriate aldehyde with the C_{12}-alkoxyaniline following literature procedures.[52] The vanadyl (IV) complexes, VOL_2 (L = salicylaldimines) were synthesized by the interaction of hot ethanolic solution of the ligands and vanadyl sulfate in the presence of triethylamine under reflux (**Scheme 3**). The bidentate [N, O] donor Schiff base ligands are abbreviated as 4-n-$OC_{12}H_{25}$ and their complexes as VO-n-$OC_{12}H_{25}$ (n = 6, 8, 16, and 18).

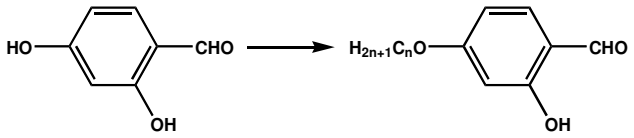

Scheme 2: $C_nH_{2n+1}Br$, $KHCO_3$, KI, dry acetone, Δ, 40 h. n = 6, 8, 16, 18

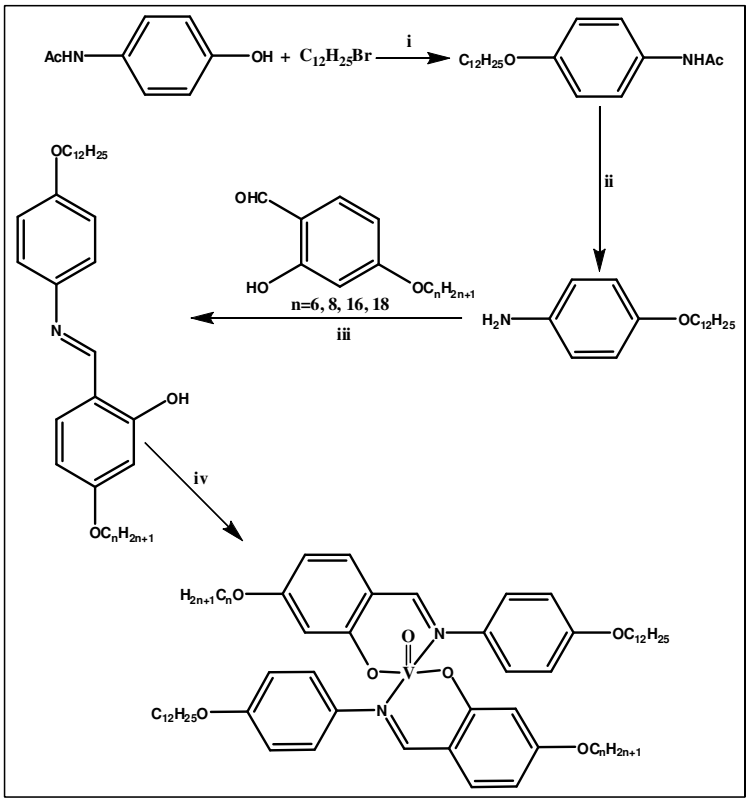

Scheme 3: i. Dry K_2CO_3, dry acetone, KI ii. H^+/H_2O, EtOH iii. Glacial acetic acid, EtOH, reflux, 2h iv. $VOSO_4.2H_2O$, TEA, Methanol reflux 1h.

Synthesis of n-alkoxysalicyldehyde (n = 6, 8, 16, and 18):

Alkoxysalicyldehyde derivatives were prepared following the general method described in literature. 2,4-Dihydroxybenzaldehyde (10mmol, 1.38g), $KHCO_3$ (10mmol, 1g), KI (catalytic amount) and 1-bromohexane (10mmol, 1.6g), 1-bromoctane (10mmol, 1.9g), 1-bromohexadecane (10mmol, 3.0g) or 1-bromo-octadecane (10mmol, 3.3g) were mixed in 250mL of dry acetone. The mixture was heated under reflux for 24h, and then filtered, while hot, to remove any insoluble solids. Dilute HCl was added to neutralize the warm solution, which was then extracted with chloroform (100mL). The combined chloroform extract was concentrated to give a purple solid. The solid was purified by column chromatography using a mixture of chloroform and hexane (v/v, 1/1) as eluent. Evaporation of the solvents afforded a white solid product (**Scheme 2**).

Synthesis of dodecyloxyaniline:

p-Hydroxy acetanilide(5g, 0.03mol) is refluxed with equimolar amount of dodecylbromide (7.5g, 0.03mol for 36h in dry acetone using 4.6g of K_2CO_3) as the base and KI as the catalyst, acetone was then dried off and the product was dissolved in CH_2Cl_2 and the solution was washed with saturated NaCl solution. The solution was then treated with Na_2SO_4 to absorb the moisture present in the solution. CH_2Cl_2 was then distilled off to obtain the crude 4-dodecyloxy acetanilide. 4-dodecyloxy acetanilide was then hydrolysed for 4h with 35% HCl in ethanol. The solution was then treated with $2moldm^{-3}$ of NaOH solution and a large amount of water upto pH=12. The product was then filtered, recrystallised with alcohol using animal charcoal to remove any colored impurity present. The synthetic route is shown in **Scheme 3.**

Synthesis of ligand N-(4-n-octadecyloxysalicylidene)-4$^{/}$-n-dodecyloxy aniline (4-18-$OC_{12}H_{25}$):

An ethanolic solution of (4-n-octadecyloxy)-salicyaldehyde (0.3g, 1mmol) was added to an ethanolic solution of 4-dodecyloxy aniline (0.3g, 1mmol). The solution mixture was refluxed with few drops of acetic acid as catalyst for 3h to yield the Schiff base N-(4-n-octadecyloxysalicylidene)-4$^{/}$-n-dodecyloxy aniline. The solid was collected by filtration and recrystallised several times from absolute ethanol to give a pure compound.

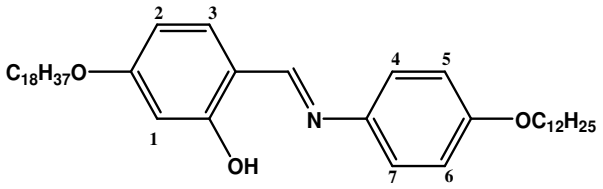

Yield: 0.37g, 75%. Anal. Calcd for $C_{43}H_{71}NO_3$: C, 79.4; H, 11.0; and N, 2.1. Found: C, 79.5%; H, 11.1%; and N, 2.2%; FAB mass (*m/e*, fragment): *m/z*: calcd 649.5; found: 650[M+H$^+$]; ^{1}H NMR (400MHz, $CDCl_3$): 0.87(t, J=6.3 Hz, 6H, –CH3), 1.2–1.5 (m, 52H, $(CH_2)_{26}$), 3.9(q, J=6.3, 4H, OCH_2), 6.4(s, 1H), 6.4(d, 8.4 Hz, 2H), 6.9(d, 8.7 Hz, 6H), 7.2(d, 8.7Hz, 3H), 7.2(d, 8.7Hz, 4, 7H), 8.5(s, 1H, CH=N), and 13.9(s, 1H, OH); ^{13}C NMR (75.45 MHz; $CDCl_3$; Me_4Si at 25°C, ppm) δ=102.4 (–C1), 107.2 (–C2), 132.4 (–C3), 122.5 (–C4), 115.8 (–C5), 115.8 (–C6), 122.5(–C7); IR (ν_{max}, cm^{-1}, KBr): 3435(–OH), 2917($\nu_{as(C–H),}$ CH_3), 2919($\nu_{as(C–H),}$ CH_2), 2869($\nu_{s(C–H),}$ CH_3), 2845($\nu_{as(C–H),}$ CH_2), 1630($\nu_{C=N}$), and 1278($\nu_{C–O}$).

N-(4-n-hexadecyloxysalicylidene)-4′-n-dodecyloxy aniline (4-16-$OC_{12}H_{25}$):

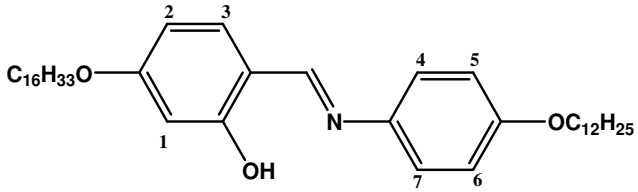

Yield: 0.38g, 76%. Anal. Calcd for $C_{41}H_{67}NO_3$: C, 79.1; H, 10.8; and N, 2.2. Found: C,79.2%; H, 10.7%; and N, 2.1%; FAB mass (*m/e*, fragment): *m/z*: calcd 621.5; found: 622[M+H$^+$]; ^{1}H NMR (400MHz, $CDCl_3$): 0.89(t, J=6.3 Hz, 6H, –CH3), 1.2–1.5 (m, 48H, $(CH_2)_{24}$), 3.8(q, J=6.3, 4H, OCH_2), 6.5(s,1H), 6.4(d, 8.4 Hz, 2H), 6.9(d, 8.7 Hz, 5, 6H), 7.2(d, 8.7 Hz, 3H), 7.6(d, 8.7 Hz, 4, 7H), 8.5(s, 1H, CH=N), and 13.9(s, 1H, OH); ^{13}C NMR (75.45 MHz; $CDCl_3$; Me_4Si at 25°C, ppm) δ=102.4 (–C1), 107.2 (–C2), 133.4(–C3), 121.5 (–C4), 115.8 (–C5), 115.8 (–C6), 122.5(–C7); IR (ν_{max},, cm^{-1}, KBr): 3435(–OH), 2917($\nu_{as(C–H),}$ CH_3), 2919($\nu_{as(C–H),}$ CH_2), 2868($\nu_{s(C–H),}$ CH_3), 2842($\nu_{as(C–H),}$ CH_2), 1631(νC=N), and 1278($\nu_{C–O}$).

N-(4-n-octyloxysalicylidene)-4′-n-dodecyloxy aniline (4-8-$OC_{12}H_{25}$):

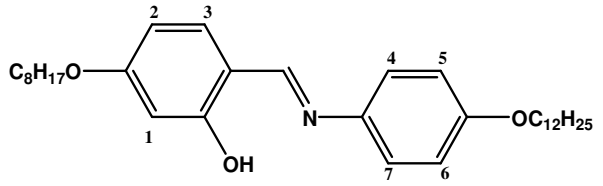

Yield: 0.33g, 75%. Anal. Calcd for $C_{33}H_{51}NO_3$: C, 77.7; H, 10.0; and N, 2.7. Found: C, 77.6%; H, 10.1%; and N, 2.6%; FAB mass (*m/e*, fragment): *m/z*: calcd 509.3; found: 510[M+H$^+$]; ^{1}H NMR (400MHz, $CDCl_3$): 0.89(t, J=6.3 Hz, 6H, –CH3), 1.2–1.4 (m, 32H, $(CH_2)_{16}$), 3.8(q, J=6.3, 4H, OCH_2), 6.5(s,1H), 6.4(d, 8.4 Hz, 2H), 6.9(d, 8.7 Hz, 5,6H), 7.2(d, 8.7 Hz, 3H), 7.5(d, 8.7 Hz, 4, 7H), 8.4(s, 1H, CH=N), 13.9(s, 1H, OH); ^{13}C NMR (75.45 MHz; $CDCl_3$; Me_4Si at 25°C, ppm) δ=102.4 (–C1), 107.2 (–C2), 133.4 (–C3), 121.5 (–C4), 115.8 (–C5), 115.8 (–C6), 122.5(–C7);IR (ν_{max}, cm^{-1}, KBr): 3435(–OH), 2917($\nu_{as(C–H),}$ CH_3), 2919($\nu_{as(C–H),}$ CH_2), 2868($\nu_{s(C–H),}$ CH_3), 2842($\nu_{as(C–H),}$ CH_2), 1631($\nu_{C=N}$), and 1277($\nu_{C–O}$).

N-(4-n-hexyloxysalicylidene)-4$^/$-n-dodecyloxy aniline (4-6-$OC_{12}H_{25}$):

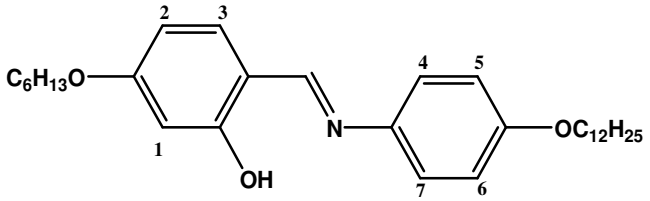

Yield: 0.33g, 75%. Anal. Calcd for $C_{31}H_{47}NO_3$: C, 77.2; H, 9.8; and N, 2.9. Found: C, 77.3%; H, 9.7%; and N, 2.8%; FAB mass (*m/e*, fragment): *m/z*: calcd 481.3; found: 482[M+H$^+$]; ^{1}H NMR (400MHz, $CDCl_3$): 0.91(t, J=6.3 Hz, 6H, –CH_3), 1.2–1.4 (m, 28H, $(CH_2)_{14}$), 3.7(q, J=6.3, 4H, OCH_2), 6.5(s, 1H), 6.5(d, 8.4 Hz,2H), 6.9(d, 8.7 Hz, 5, 6H), 7.3(d, 8.7 Hz, 3H), 7.5(d, 8.7 Hz, 4, 7H), 8.4(s, 1H, CH=N), and 13.9(s, 1H, OH); ^{13}C NMR (75.45 MHz; $CDCl_3$; Me_4Si at 25°C, ppm) δ=102.4 (–C1), 107.2 (–C2), 133.4 (–C3), 121.5 (–C4), 115.8 (–C5), 115.8 (–C6), and 122.5(–C7); IR (ν_{max}, cm^{-1}, KBr):3435(–OH), 2917($\nu_{as(C–H),}$ CH_3), 2918($\nu_{as(C–H),}$ CH_2), 2867($\nu_{s(C–H),}$ CH_3), 2842($\nu_{as(C–H),}$ CH_2), 1632($\nu_{C=N}$), and 1277($\nu_{C–O}$).

Synthesis of oxovanadium (IV) complexes:

To the ligand 4-18-$OC_{12}H_{25}$ (0.64g, 1mmol) or 4-16-$OC_{12}H_{25}$ (0.62g, 1mmol) or 4-8-$OC_{12}H_{25}$ (0.50g, 1mmol) and 4-6-$OC_{12}H_{25}$ (0.48g, 1mmol) dissolved in minimum volume of absolute ethanol vanadyl sulfate $VOSO_4.2H_2O$ (0.11g, 0.5mmol) in methanol was added followed by addition of triethylamine and refluxed for 2 h. A greenish solid formed immediately was filtered, washed with diethyl ether and recrystallised from chloroform–ethanol.

Complex (VO-18-$OC_{12}H_{25}$):

Yield: 0.56g (75%) Anal. Calcd for $C_{86}H_{140}N_2O_7V$: C, 75.6; H, 10.3; and N, 2.0. Found: C, 75.5%; H, 10.4%; and N, 2.1%; FAB mass (*m/e*, fragment): *m/z*: calcd 1364.0; found: 1365[M+H^+]; IR (ν_{max}, cm^{-1}, KBr): 1616($\nu_{C=N}$), 1132 (ν_{C-O}, phenolic), and 970($\nu_{V=O}$).

Complex, (VO-16-$OC_{12}H_{25}$):

Yield: 0.56g (78%) Anal. Calcd for $C_{82}H_{132}N_2O_7V$: C, 75.2; H, 10.1; and N, 2.1. Found: C, 75.1%; H, 10.2%; and N, 2.0%; FAB mass (*m/e*, fragment): *m/z*: calcd 1307.0; found: 1308[M+H^+]; IR (ν_{max}, cm^{-1}, KBr): 1612($\nu_{C=N}$), 1135 (ν_{C-O}, phenolic), and 969($\nu_{V=O}$).

Complex, (VO-8-$OC_{12}H_{25}$):

Yield: 0.45g (76%) Anal. Calcd for $C_{66}H_{100}N_2O_7V$: C, 73.1; H, 9.2; and N, 2.5. Found: C, 73.2%; H, 9.3%; and N, 2.4%; FAB mass (*m/e*, fragment): *m/z*: calcd 1083.7; found: 1084[M+H^+]; IR (ν_{max}, cm^{-1}, KBr): 1611($\nu_{C=N}$), 1134 (ν_{C-O}, phenolic), and 970($\nu_{V=O}$).

Complex, (VO-6-$OC_{12}H_{25}$):

Yield: 0.44g (75%) Anal. Calcd for $C_{62}H_{92}N_2O_7V$: C, 72.4; H, 9.0; and N, 2.7. Found: C, 72.3%; H, 9.1%; and N, 2.6%; FAB mass (*m/e*, fragment): *m/z*: calcd 1027.6; found: 1028[M+H^+]; IR (ν_{max}, cm^{-1}, KBr): 1614($\nu_{C=N}$), 1133(ν_{C-O}, phenolic), and 971($\nu_{V=O}$).

3.2.2.1 Result and discussion:

Synthesis and structural assessment:

The synthetic procedure for ligands and metal complexes are depicted in **Scheme 2 and Scheme 3**. The Schiff base ligands were synthesized by literature procedures.[23,40] The characterization of the compounds was made by elemental analyses, FT-IR, UV-Vis, ^1H NMR, ^{13}C NMR and mass spectrometry. The analytical data are in good agreement with the proposed formulae. A strong band observed at ~1622-1624cm^{-1} in the IR spectrum is assigned to $\nu_{(C=O)}$. The IR spectra of the free ligands exhibit the characteristic bands of imine(C=N), which appear at ~1630cm^{-1}. In metal complexes the $\nu_{(CN)}$ band is generally shifted to lower wave numbers relative to the free ligand indicating a decrease in the C=N bond order due to the coordination of the imine

nitrogen to the metal and back bonding from the VO(IV) center to the π* orbital of the azomethine group.[36] Moreover, the absence of ν_{OH} mode at ~3155cm^{-1} indicated its coordination to VO(IV) center. The $\nu_{C=N}$ stretching is rather independent of the length of alkoxy side chain. Occurrence of vanadyl (V=O) stretching mode at *ca* 970cm^{-1} evidenced the absence of any intermolecular (·····V=O·····V=O·····) interaction attesting the monomeric nature of the complexes.[29] Appearance of additional bands at ~450-480 and ~527-549cm^{-1} in the spectra of the complexes assigned to the V–O and V–N stretching vibrations that are not observed in the spectra of the ligands furnished evidence for [N,O] binding mode of the ligand. The ^{1}H NMR spectra of ligands showed signal at 13.4-13.8ppm, corresponding to the proton of the OH group. The imine group appears at 8.5ppm. The FAB-mass spectra of the vanadyl(IV) complexes are concordant with their formula weights. The electronic spectra (**Fig.25**) of the ligands and their complexes were recorded in dichloromethane (Table 5). The ligand exhibited two absorption bands centered at ~285 and ~350nm, attributed to π-π* transition localized on the aromatic rings. Upon complexation, these bands are red shifted to ~315 and ~385nm. In addition, complexes displayed a band at ~465nm, owing to the LMCT transition.[38]

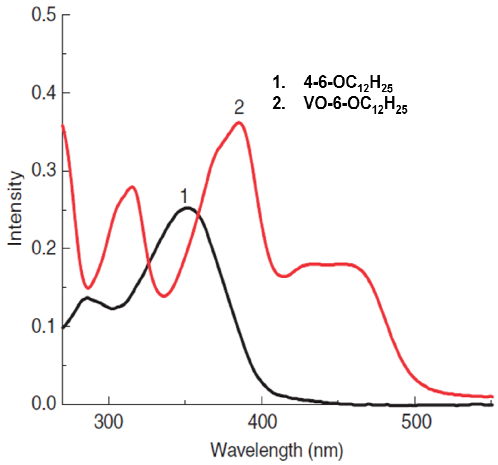

Fig. 25: UV-Vis spectra of 4-6-$OC_{12}H_{25}$ and VO-6-$OC_{12}H_{25}$

Table 5: Spectral data of the compounds:

Compounds	**UV-vis, λ_{max}(nm) (ϵ, l mol^{-1} cm^{-1}) (Transition)**	**IR(cm^{-1})**	**FAB Mass**
$C_{43}H_{71}NO_3$ (4-18-$OC_{12}H_{25}$)	286(1360) ($\pi\rightarrow\pi^*$)	1630($\nu_{C=N}$)	650
	349(2530) ($\pi\rightarrow\pi^*$)	3431(ν_{OH})	
$C_{86}H_{140}N_2O_7V$ (VO-18-$OC_{12}H_{25}$)	315(2750) ($\pi\rightarrow\pi^*$)	1616($\nu_{C=N}$)	622
	385(3590) ($\pi\rightarrow\pi^*$)	970($\nu_{V=O}$)	
	446(1800) (LMCT)	532(ν_{M-N})	
		461(ν_{M-O})	
$C_{41}H_{67}NO_3$ (4-16-$OC_{12}H_{25}$)	284(1350) ($\pi\rightarrow\pi^*$)	1631($\nu_{C=N}$)	510
	350(2530) ($\pi\rightarrow\pi^*$)	3433(ν_{OH})	
$C_{82}H_{132}N_2O_7V$ (VO-16-$OC_{12}H_{25}$)	315(2745) ($\pi\rightarrow\pi^*$)	1612($\nu_{C=N}$)	482
	381(2750) ($\pi\rightarrow\pi^*$)	970($\nu_{V=O}$)	
	441(1950) (LMCT)	531(ν_{M-N})	
		457(ν_{M-O})	
$C_{33}H_{51}NO_3$(4-8-$OC_{12}H_{25}$)	282(1350) ($\pi\rightarrow\pi^*$)	1632($\nu_{C=N}$)	1365
	352(2730) ($\pi\rightarrow\pi^*$)	3432(ν_{OH})	
$C_{66}H_{100}N_2O_7V$(VO-8-$OC_{12}H_{25}$)	317(2550) ($\pi\rightarrow\pi^*$)	1611($\nu_{C=N}$)	1308
	379(1750) ($\pi\rightarrow\pi^*$)	969($\nu_{V=O}$)	
	438(1640) (LMCT)	532(ν_{M-N})	
		458(ν_{M-O})	
$C_{31}H_{47}NO_3$ (4-6-$OC_{12}H_{25}$)	285(1350) ($\pi\rightarrow\pi^*$)	1632($\nu_{C=N}$)	1084
	350(2630) ($\pi\rightarrow\pi^*$)	3431(ν_{OH})	
$C_{62}H_{92}N_2O_7V$(VO-6-$OC_{12}H_{25}$)	315(2450) ($\pi\rightarrow\pi^*$)	1614($\nu_{C=N}$)	1228
	385(1450) ($\pi\rightarrow\pi^*$)	971($\nu_{V=O}$)	
	446(1560) (LMCT)	531(ν_{M-N})	
		453(ν_{M-O})	

Variable temperature magnetic susceptibility study:

The temperature dependence of the magnetic susceptibilities is carried out for VO-18-$OC_{12}H_{25}$ in the temperature range 2.5-300K under a 1 kOe applied field. The effective magnetic moment for a typical complex VO-18-$OC_{12}H_{25}$ is found to be 1.73 B.M. The χ_M^{-1} versus T-plot is almost linear down to 30K and then decreases with increase of temperature. The inverse of the susceptibility plotted against temperature (**Fig.26**), satisfies the Curie–Weiss equation. The strength of efficient superexchange path is presumably hindered by coordinating ability of the metal ion. The vanadium complexes can thus be considered as magnetically isolated spin (d^1) centers. Absence

of any maximum in χ_M *versus* T indicated nonexistence of strong exchange interactions between the spin centers.

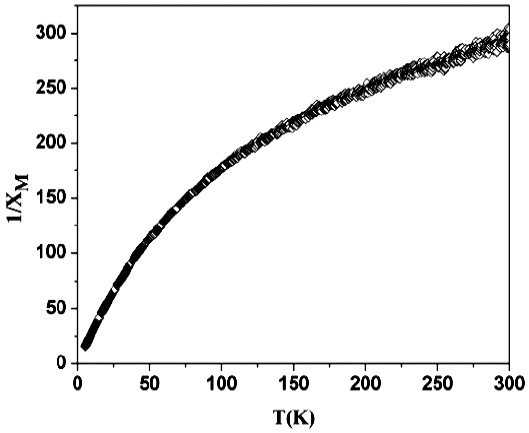

Fig. 26: Variation of magnetic susceptibility of VO-18-$OC_{12}H_{25}$ with temperature.

Electrochemical behaviour:

The redox behavior of a representative VO-16-$OC_{12}H_{25}$ complex was probed by cyclic voltammetry in dichloromethane solution in the potential range –4.0 to 1.4V *versus* SCE at a scan rate of $0.05Vs^{-1}$. The voltammogram (**Fig.27**) displayed a quasireversible (peak separation >100mV) one-electron response. The peak separation ($E_{1/2}$ = +0.57, E_{pc} = -0.14V, Ep^a = 1.0V, ΔE_p = 0.86V) is assigned to VO^{3+}/VO^{2+} couple. On scanning to negative potential, no response is observed implying redox innocent characteristics of the ligand, supported also by the free ligand cyclic voltammetry.

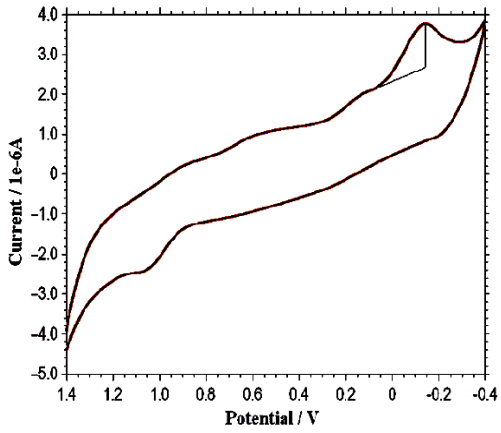

Fig. 27: Cyclic voltammogram of VO-16-$OC_{12}H_{25}$

Mesomorphic behaviour: polarising optical microscopy and DSC studies:

The liquid crystalline behavior of all the compounds was monitored by DSC studies and polarizing optical microscopy (POM). The phase transitions and thermodynamic data are summarized in Table 6. The compounds are all found to be mesomorphic. All the ligands exhibited enantiotropic phase transitions. Upon cooling the sample from isotropic liquid, a schlieren texture of SmC phase (**Fig.28**) with four brush defect at 110-125°C was observed. The DSC trace for the lower homologues (6-$OC_{12}H_{25}$ and 8-$OC_{12}H_{25}$) showed two transitions in heating and two in cooling cycle. However, in case of higher homologues (16-$OC_{12}H_{25}$ and 18-$OC_{12}H_{25}$), in addition to smectic mesophase, a crystal to crystal transition is observed in heating cycles (**Fig.29**) which could not be detected in POM study. The mesophase to isotropic transition temperature decreases with increase in chain length. The variation of transition temperature with carbon chain length is shown in **Fig.30**. The oxovanadium(IV) complexes showed SmA/SmX phases. In polarizing optical microscopic study, cooling the samples from isotropic liquid, typical batonnets are formed which coalesce to give rise to a highly birefringent fanlike texture, characteristic of the smectic A phase (**Fig.31**). On further cooling, the sample an arced like texture observed for all the complexes was diagnostic of unidentified SmX phase (**Fig.32**). The DSC trace (**Fig.33**) for a representative compound VO-18-$OC_{12}H_{25}$ exhibited two transitions both in heating and cooling cycles. Moreover at 73°C, a glass transition could be observed for the complex in heating run. The variations in transition temperatures as a function of carbon chain length are depicted in **Fig.34**. No definitive trend was found to emerge as a function of carbon chain length variation. The isotropisation temperatures were, however, mostly decreased with increasing carbon chain length.

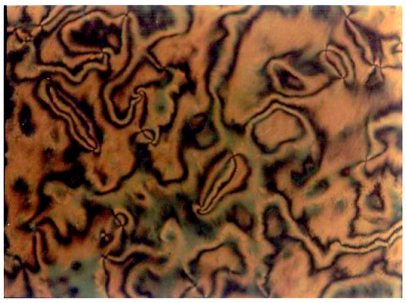

Fig. 28: Schlieren texture of SmC phase

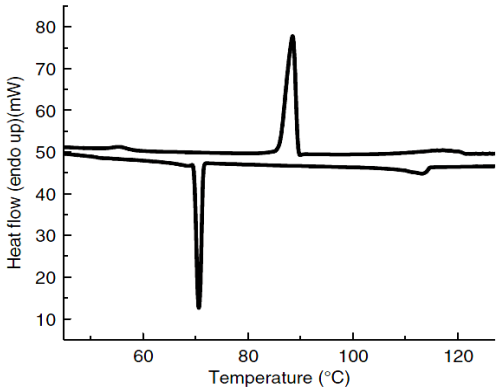

Fig. 29: DSC thermogram of 4-16-$OC_{12}H_{25}$

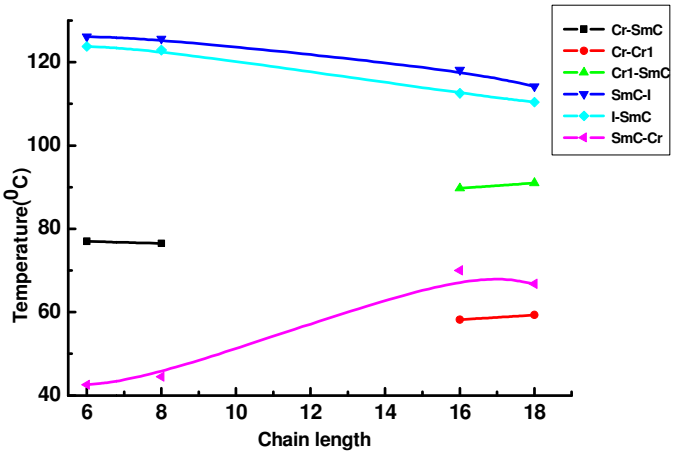

Fig. 30: Variation of transition temperature with carbon chain length in ligands

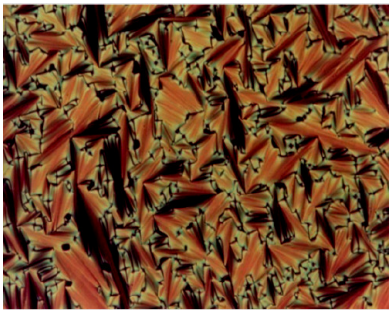

Fig. 31: Fanlike texture of SmA phase.

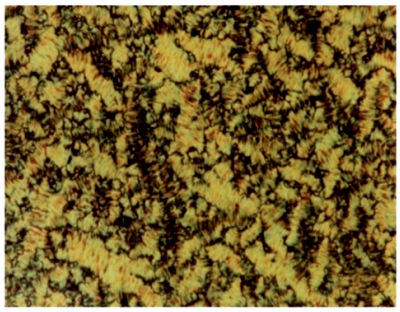

Fig. 32: Unidentified SmX phase.

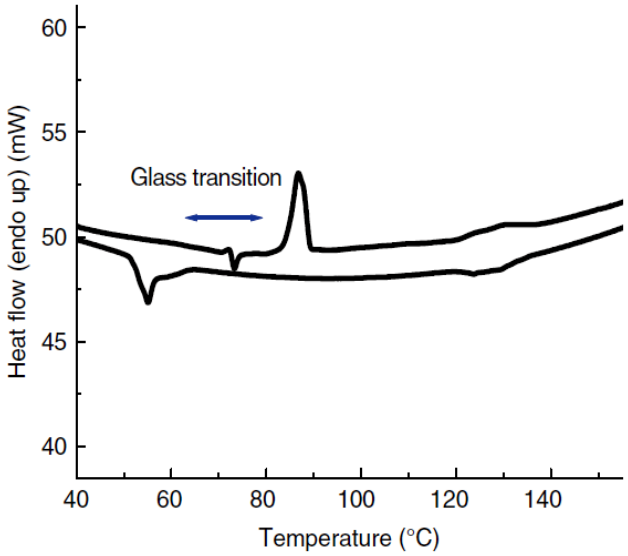

Fig.33: DSC thermogram of VO-18-$OC_{12}H_{25}$.

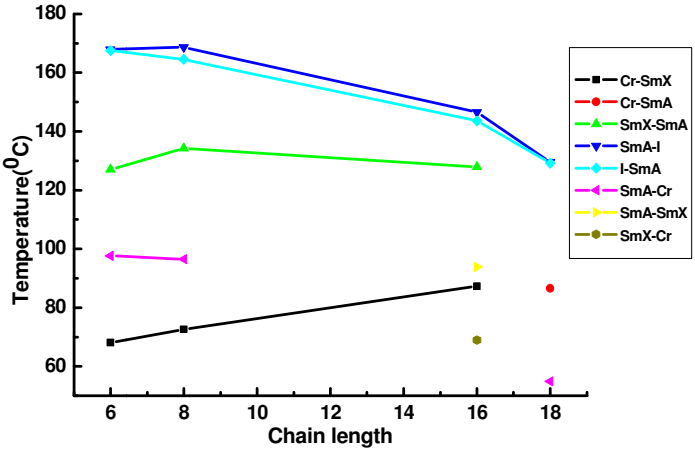

Fig. 34: Variation of transition temperature with carbon chain length in complexes.

Table 6: Phase transitions temperatures (T°C), associated enthalpies (ΔH, kJ mol^{-1}) of the compounds.

Compounds	Heating	Cooling
4-6-$OC_{12}H_{25}$	Cr 77.0(40.2)SmC126.1(6.7)I	I123.8(6.0)SmC42.6 (15.6)Cr
4-8-$OC_{12}H_{25}$	Cr 76.5(49.0) SmC 125.6(7.9)I	I122.9(7.5)SmC44.5 (23.8)Cr
4-16-$OC_{12}H_{25}$	Cr58.2(2.1)Cr189.7(71.2) SmC118.1(6.6)I	I117.5(4.8) SmC70.0(47.7)Cr
4-18-$OC_{12}H_{25}$	Cr59.3(1.9)Cr191.0(74.6)SmC 114.2(6.3)I	I110.4(4.3)SmC 66.8(71.4)Cr
VO-6-$OC_{12}H_{25}$	Cr68.1(2.9)SmE127(4.3) SmA167.9(5.9)I	I167.5(3.9)SmA97.7 (4.9)Cr
VO-8-$OC_{12}H_{25}$	Cr72.6(2.2)SmE134.2(5.3) SmA168.7(5.4)I	I164.5(4.6)SmA96.5 (4.2)Cr
VO-16-$OC_{12}H_{25}$	Cr87.3(16.7)SmE127.9(15.5) SmA146.5(11.6)I	I143.6(9.5)SmA93.9 (20.9) SmE69.0(6.6)Cr
VO-18-$OC_{12}H_{25}$	Cr86.6(61.8)SmA129.5(11.8)I	I129.2(14.0)SmA54.9 (31.2)Cr

Density functional theory study:

As X-ray quality crystals could not be grown, density functional theory (DFT) studies were carried out to ascertain the energy optimized structures. Geometry optimization of a representative complex, VO-6-$OC_{12}H_{25}$ (**Fig.35**) has been performed without applying any symmetry constrain within the generalized gradient approximation level using the Becke–Lee–Yang–Parr (BLYP)[48] exchange and correlation functional implemented in the DMol3.[49] The DNP basis set chosen in this study is a double-numerical atomic orbital augmented by polarization functions.[53] The DNP basis set is comparable to 6-31G** Gaussian basis sets with a better accuracy for a similar basis set size due to core electron inclusion. The global cut off radius is set to be 5.0A°. The convergence criteria for energy, force and displacement were 1×10^{-5} hartree, 2×10^{-3} hartree/A°, and $5\times10^{-3}A^{\circ}$ respectively. The 3-D isosurface plots of the lowest unoccupied molecular orbital (LUMO) and the highest occupied molecular orbital (HOMO) of the complex are shown in **Fig.36** and **Fig.37**. The energies of the HOMO and LUMO of the VO(IV) complex derived from DFT are found to be -3.887 and -2.310 eV, respectively (ΔE = 1.577eV). The electron density of the LUMO is localized mainly on the C–N bonds while the HOMO is predominantly C–O bond

orbitals. Geometric parameters of the optimized VO(IV) complex are furnished in Table 7. The average V–O and V–N bond lengths are 1.95 and 2.18A° respectively. The bond length between oxido ligand and vanadium is evaluated to be 1.623A°. The bond angles varied from 86.2° to 161.7°, respectively, suggesting a distorted square pyramidal geometry around the vanadyl(IV) center.

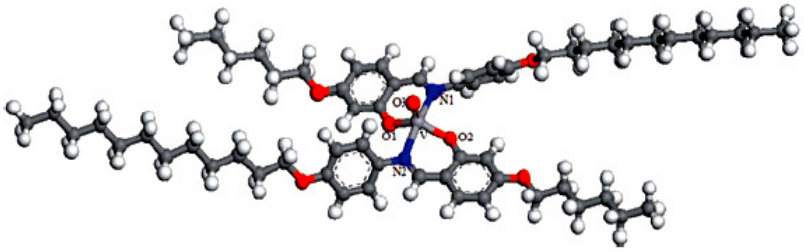

Fig. 35: Optimized structure of VO-6-$OC_{12}H_{25}$

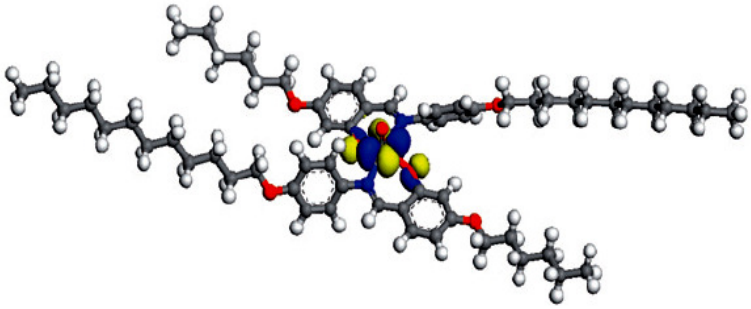

Fig. 36: HOMO of VO-6-$OC_{12}H_{25}$

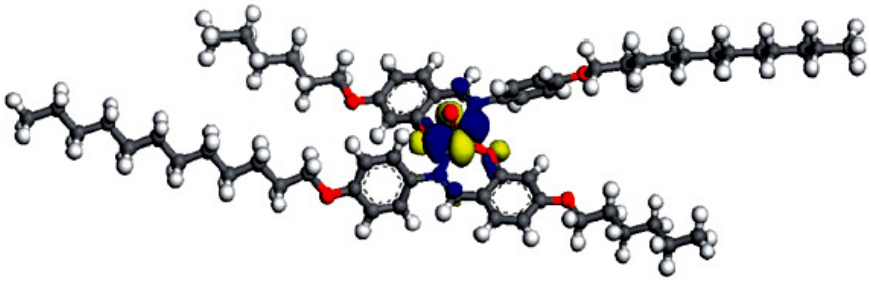

Fig. 37: LUMO of VO-6-$OC_{12}H_{25}$

Table 7: Selected bond lengths (A˚) and bond angles (°C) of VO-6-$OC_{12}H_{25}$ complex optimized at the BLYP/DNP level of theory.

Structure parameter	VO-6-$OC_{12}H_{25}$
V–O(1)	1.952
V–O(2)	1.956
V–O(3)	1.622
V–N(1)	2.182
V–N(2)	2.181
O(1)–V–O(2)	130.4
N(1)–V–N(2)	161.7
N(1)–V–O(2)	86.2
O(1)–V–N(1)	84.1
O(1)–V–N(2)	86.1
N(2)–V–O(2)	86.4

3.3 Conclusion:

Two series of oxovanadium(IV) and copper(II) salicylaldimine complexes bearing polar substituent on aromatic rings have been successfully synthesised. The mesomorphic properties of the compounds are strongly dependent on substituent as well as on carbon chain length. The ligands are found to exhibit smectic/nematic mesomorphism. However, nitro substituent compounds with C_4 tail lack any mesomorphism. None of the oxovanadium complexes are found to be mesogenic. Interestingly, the copper complexes except the nitro substituted one (C_4 tail) are mesogenic and showed smectic A phase at >200°C. Cyclic voltammetry study revealed a quasireversible one-electron response for all the complexes. Variable temperature magnetic susceptibility studies suggested occurrence of isolated spin centers with hardly any exchange interaction. The $\nu_{V=O}$ band at ~980cm^{-1} also suggested lack of any discernible …V=O.....V=O… interaction. Based on spectral and DFT studies a tentative five coordinate square pyramidal for vanadium- and a square planar structure for copper-complexes has been proposed.

Successful synthesis of a series of new oxovanadium(IV) complexes bearing long as well as short alkoxy tail on both side of aromatic ring has been demonstrated. All the compounds are found to exhibit smectic mesomorphism. No definitive trends were noted as a function of carbon chain lengths of alkoxy tails both for the ligands and

complexes. Cyclic voltammetry study revealed a quasireversible one-electron response for the VO(V)/VO(IV) redox couple. The compounds are all found to be thermally quite stable. Based on DFT, spectral and magnetic studies, a distorted square pyramidal five-coordinate structure have been proposed. The synthetic strategy adopted herein can be effectively employed to access newer mesogenic vanadyl complexes.

References:

1. Chohan, Z. H.; Sumrra, S. H.; Youssoufi, M. H.; Hadda, T. B. *J. Coord. Chem.* **2010**, *63*, 3981.
2. Abe, Y.; Iyoda, A.; Seto, K.; Moriguchi, A.; Yokoyama, H. *Eur. J. Inorg. Chem.* **2008**, 2148.
3. Bagherzadeh, M.; Amini, M. *J. Coord. Chem.* **2010**, *63,* 3849.
4. Sarkar, S.; Dey, K.; Biswas, S.; Bhaumik, B. B. *J. Coord.Chem.* **2007**, *60* 1143.
5. Mohebbi, S.; Bakhshi, B. *J. Coord. Chem.* **2008**, *61*, 2615.
6. Patel, K. S.; Bailar, J. C. Jr. *J. Coord. Chem.* **1973**, *3*, 113.
7. Date, R.W.; Bruce, D. W. *Liq. Cryst.* **2004**, *31*, 1435.
8. Espinet, P.; Esteruelas, M. A.; Oro, L. A.; Serrano, J. L.; Sola, E. *Coord. Chem. Rev.***1992**, *117*, 215.
9. Giroud-Godquin, A. M.; Maitlis, P. M. *Angew. Chem., Int. Ed.* **1991**, *30*, 375.
10. Hoshino, N. *Coord. Chem. Rev.* **1998**,*174*, 77.
11. Lai, C. K.; Chang, C. H.; Tsai, C. H. *J. Mater. Chem.* **2007**, *17*, 2319.
12. Barbera, J.; Levelut, A.M.; Marcos, M.; Romero, P.; Serrano, J. L. *Liq. Cryst.* **1991**, *10*, 119.
13. Barbera, J.; Gimenez, R.; Gimeno, N.; Marcos, M.; Pina, M. D. C.; Serrano, J. L. *Liq. Cryst.* **2003**, *30*, 651.
14. Chou, S. Y.; Chen, C. J.; Tsai, S. L.; Sheu, H. S.; Lee, G. H.; Lai, C.K. *Tetrahedron* **2009**, *65*, 1130.
15. Abe, Y.; Iyoda, A. Seto, K. Moriguchi, A.; Tanase, T.; Yokoyama, H. *Eur. J. Inorg. Chem.* **2008**, 2148.
16. Glebowska, A.; Przybylski, P.; Winek, M.P.; Krowczynski, A.; Szydlowska, Z.; Pociecha, D.; Gorecka, E. *J. Mater. Chem.* **2009**, *19*, 1395.
17. Szydlowska, J.; Krowczynski, A.; Gorecka, E.; Pociecha, D. *Inorg. Chem.* **2000**, *39*, 4879.
18. Caruso, U.; Diana, R.; Panunzi, B.; Roviello, A.; Tingoli, M.; Tuzi, A. *Inorg. Chem. Commun.* **2009**, *12*, 1135.
19. Singh, A. K.; Kumari, S.; Rao, T. R.; Mater. *Sci. Eng. C* **2011**, *31*, 1144.
20. Zheng, H.; Lai, C. K.; Swager, T. M. *Chem. Mater.* **1995**, *7*, 2067.

21. Barbera, J.; Gimenez, R.; Serrano, J.L.; Alonso, P.J.; Martinez, J. I. *Chem. Mater.* **2003**, *15*, 958.
22. Abe, Y.; Nakabayashi, K.; Matsukawa, N.; Takashima, H.; Iida, M.; Tanase, T.; Sugibayashi, M.; Mukai, H.; Ohta, K. *Inorg. Chim. Acta.* **2006,** *359*, 3934.
23. Bhattacharjee, C. R.; Das, G.; Purkayastha, D. D.; Mondal, P.; Kanoo. P. *J. Coord. Chem.* **2011**, *64*, 2746.
24. Wang, C. S.; Wang, I. W.; Cheng, K. L.; Lai, C. K. *Tetrahedron* **2006**, *62*, 9383.
25. Eran, B. B.; Yorur, C.; Tschierske, C.; Prehm, M.; Baumeister, U. *J. Mater. Chem*. **2007**, *17*, 2319.
26. Duan, M.; Tasaka, T.; Okamoto, H.; Petrov, V. F.; Takenaka, S. *Liq. Cryst.* **2000**, *27*, 1195.
27. Filippov, S. K.; Kolomiets, I. P.; Sokolova, O. S.; Antonov, E. A.; Zorin, I. M.; Bilibin, A. Y. *Liq. Cryst.* **1998**, *24,* 787.
28. Yeap, G. Y.; Ha, S.-T.; Lim, P. L.; Boey, P. L.; Ito, M. M.; Sanehisa, S.; Youhei, Y. *Liq. Cryst.* **2006**, *33*, 205.
29. Espinet, P.; Esteruelas, M. A.; Oro, L. A.; Serrano, J. L.; Sola, E. *Coord. Chem. Rev.* **1992**, *117*, 215.
30. Hudson, S. A.; Maitlis, P. M. *Chem. Rev.* **1993**, *93,* 861.
31. Prajapati A. K.; Bonde, N. *Liq. Cryst.* **2006**, *33*, 1189.
32. Rezvani, Z.; Nejati, K.; Seyedahmadian, M.; Divband, B. *Mol. Cryst. Liq. Cryst.* **2008**, *493*, 71.
33. Mocanu, A. S.; Ilis, M.; Dumitrascu, F.; Ilie, M.; Circu, V. *Inorg. Chim. Acta.* **2010**, *363*, 729.
34. Caruso, U.; Diana, R.; Panunzi, B.; Roviello, A.; Tingoli, M.; Tuzi, A. *Inorg. Chem.Commun.* **2009**, *12*, 1135.
35. Hayami, S.; Danjobara, K.; Miyazaki, S.; Inoue, K.; Ogawa, Y.; Maeda, Y. *Polyhedron* **2005**, *24*, 2821.
36. Kadkin, O. N.; Kim, E. H.; Rha, Y. J.; Kim, S. Y.; Tae, J.; Choi, M. G. *Chem. Eur. J.* **2009**, *15,* 10343.
37. Hayami, S.; Motokawa, N.; Shuto, A.; Masuhara, N.; Someya, T.; Ogawa, Y.; Inoue, K.; Maeda, Y. *Inorg. Chem.* **2007**, *46,* 1789.

38. Morale, F.; Finn, R. L.; Collinson, S. R.; Blake, A. J.; Wilson, C.; Bruce, D. W.; Guillon, D.; Donnio, B.; Schroder, M. *New J. Chem.* **2008**, *32*, 297.
39. Bhattacharjee, C. R.; Das, G.; Mondal, P.; Prasad, S. K.; Rao, D. S. S. *Liq. Cryst.* **2011**, *38*, 615.
40. Bhattacharjee, C. R.; Das, G.; Mondal, P. *J. Coord. Chem.* **2011**, *64*, 3273.
41. Ghedini, M.; Morrone, S.; Bartolino, R.; Formoso, V.; Francescangeli, O.; Yang, B.; Gatteschi, D.; Znachini, C. *Chem. Mater.* **1993**, *5*, 876.
42. Zheng, H.; Lai, C. K.; Swager, T. M. *Chem. Mater.* **1995**, *7,* 2067.
43. Alonso, P. J.; Sanjuan, M. L.; Romero, P.; Marcos, M.; Serrano, J. L. *J. Phys. Condens. Mater* **1990**, *2*, 9173.
44. Bhattacharjee, C. R.; Das, G.; Mondal, P.; Prasad, S. K.; Rao, D. S. S. *Inorg. Chem. Commun.* **2011**, 14, 606.
45. Chattopadhyay, T.; Mukherjee, M.; Banu, K.S.; Banerjee, A.; Suresh, E.; Zangrando, E.; Das, D. *J. Coord. Chem.* **2009,** *62,* 967.
46. Chen, X.; Yamaguchi, A.; Namekawa, M.; Kamijo, T.; Teramae, N.; Tong, A. *Anal. Chim. Acta.* **2011,** *24*, 94.
47. Lu, Y.; Liu, J.W. *J. Am. Chem. Soc.* **2007,** *129*, 9838.
48. Lee, C.; Yang, W.; Parr, R.G. *Phys. Rev. B Condens. Matter* **1988,** *37*, 785.
49. Delley, B. *J. Chem. Phys.* **1990,** *92*, 508.
50. Pearson, R. G. *J. Chem. Educ.* **1987**, *64*, 561.
51. Khandar, A. A.; Nejati, K. *Polyhedron* **2000**, *19*, 607.
52. Bhattacharjee, C. R.; Das, G.; Purkayastha, D. D.; Mondal, P. *Liq. Cryst.* **2011**, *38*, 717.
53. Suzuki, K.; Nada, T.; Sastre, G.; Katada, N.; Niwa, M. *J. Phys. Chem. C* **2009**, *113*, 5672.